Open access • Journal Article • DOI:10.1063/1.3103326

Hydrogen quantification in hydrogenated amorphous carbon films by infrared, Raman, and x-ray absorption near edge spectroscopies — Source link

Josephus Gerardus Buijnsters, Raúl Gago, I. Jimenez, M Camero ...+2 more authors

Published on: 05 May 2009 - Journal of Applied Physics (American Institute of Physics)

Topics: Raman spectroscopy, Amorphous carbon, Infrared spectroscopy, XANES and Absorption spectroscopy

Hydrogen quantification in hydrogenated amorphous carbon films by infrared, Raman, and x-ray absorption near edge spectroscopies

J. G. Buijnsters,[1,2,a)] R. Gago,[1,3] I. Jiménez,[1] M. Camero,[1] F. Agulló-Rueda,[1] and C. Gómez-Aleixandre[1]

[1]*Instituto de Ciencia de Materiales de Madrid, Consejo Superior de Investigaciones Científicas, Cantoblanco, E-28049 Madrid, Spain*

[2]*Institute for Molecules and Materials (IMM), Radboud University Nijmegen, Toernooiveld 1, 6525 ED Nijmegen, The Netherlands*

[3]*Centro de Microanálisis de Materiales, Universidad Autónoma de Madrid, Cantoblanco, E-28049 Madrid, Spain*

(Received 20 January 2009; accepted 18 February 2009; published online 5 May 2009)

In this study, we have employed infrared (IR) absorption spectroscopy, visible Raman spectroscopy, and x-ray absorption near edge structure (XANES) to quantify the hydrogen (H) content in hydrogenated amorphous carbon (*a*-C:H) films. *a*-C:H films with a hydrogen content varying from 29 to 47 at. % have been synthesized by electron cyclotron resonance chemical vapor deposition at low substrate temperatures (<120 °C) applying a wide range of bias voltage, V_b, (-300 V $< V_b < +100$ V). With the application of high negative V_b, the *a*-C:H films undergo a dehydrogenation process accompanied by a sharp structural modification from polymer- to fullerenelike films. The trend in the H content derived from elastic recoil detection analysis (ERDA) is quantitatively reproduced from the intensity of the C–H bands and states in the IR and XANES spectra, respectively, as well as from the photoluminescence (PL) background drop in the Raman spectra. Using the H contents obtained by ERDA as reference data, semiquantitative expressions are inferred for the amount of bonded hydrogen as a function of the experimental spectroscopic parameters, i.e., the integrated area of the IR C–H stretching band at about 2900 cm^{-1}, the PL background in visible Raman spectra, and the XANES intensity of the σ^*-CH peak. © *2009 American Institute of Physics*. [DOI: 10.1063/1.3103326]

I. INTRODUCTION

Hydrogen-free (*a*-C) and hydrogenated (*a*-C:H) amorphous carbon films display tunable mechanical and electrical properties together with biocompatibility and, therefore, can be found in many tribological and biomedical applications.[1] Commonly, the various *a*-C:H materials are classified considering the ternary phase diagram displaying the percentages of sp^2 and sp^3 carbon and bonded hydrogen. According to this classification,[2,3] polymerlike *a*-C:H (PLCH), diamondlike *a*-C:H (DLCH), graphitelike *a*-C:H (GLCH), and tetrahedral *a*-C:H (TACH) can be distinguished. PLCH displays the highest H content and its polymerlike structure governed by the H terminated sp^3 C hybrids results in a low density and soft matrix. DLCH is characterized by an intermediate H content and higher ratio of sp^3 C hybrids, whereas TACH can be considered as a class of DLCH with increasing number of sp^3 C at constant H content. The very high sp^3 content confers TACH superior mechanical and tribological properties.[4] Finally, GLCH combines a low H content with a high sp^2 content. Thus, the physical properties of *a*-C:H films do not only directly depend on the ratio of sp^2 (graphitelike) and sp^3 (diamondlike) carbon hybrids but also on the content of bonded H.[2] Therefore, the quantification of the H content in *a*-C:H films is of great importance. Hereto, several analysis techniques such as elastic recoil detection analysis (ERDA), nuclear magnetic resonance (NMR), nuclear reaction analysis, and thermal hydrogen evolution have been employed to quantify the hydrogen content with great accuracy.[5–7] Recently, Yubero *et al.*[6] showed that reflection electron energy loss spectroscopy (REELS) can also be employed to nondestructively determine the hydrogen content at the surface of *a*-C:H films. This method relies on the backscattering of electrons from the H atoms present at the sample surface, and analysis of the elastic peak enables the determination of the H content with an accuracy of about 10%.[6,8]

Nevertheless, there is a great demand for the use of alternative, simple, nondestructive, and preferably less costly methods such as infrared (IR) and Raman spectroscopy to quantify the H content in *a*-C:H films reliably. In this study we have employed four techniques to assess the hydrogen content in biased-enhanced electron cyclotron resonance chemical vapor deposited (ECR-CVD) *a*-C:H films. Due to its high accuracy (±2 at. %) and absolute measurements, ERDA was used as the reference method. Visible Raman and IR spectroscopies are widely employed in *a*-C:H film characterization due to their relative simplicity, nondestructive character, and low cost. Thus, their capabilities to yield H quantification are addressed in this study. In particular, spectral features such as the intensity of the sp^3 C–H bond stretching vibrations around 2900 cm^{-1} in IR spectra[9] as

a)Author to whom correspondence should be addressed. Electronic mail: j.buijnsters@science.ru.nl. Present address: Institute for Molecules and Materials (IMM), Radboud University Nijmegen, Toernooiveld 1, 6525 ED Nijmegen, The Netherlands.

well as the photoluminescence (PL) background in visible Raman spectra[10] are relative measures for the amount of hydrogen present in *a*-C:H materials. We also employed x-ray absorption near edge structure (XANES) here for its high selectivity to sp^2 and sp^3 hybrids, surface character, and for being nondestructive. We show here, for the first time, that the σ^* XANES intensity related to the C–H states at 287–290 eV is a relative measure for the content of bonded hydrogen within the *a*-C:H films. Whereas ERDA results in an absolute, quantitative analysis of the total hydrogen percentage, XANES, visible Raman, and IR absorption spectroscopy only allow a semiquantitative evaluation. To our knowledge, this is the first time that these four techniques are combined in one single study, allowing a direct comparison between them.

For this work, *a*-C:H films prepared by biased ECR-CVD have been studied. This technique can provide films within a broad range of H contents by varying the kinetic energy of the impinging ions through the dc voltage applied to the substrate. In this way, a relatively narrow ion energy distribution is obtained without significantly changing other plasma parameters.[11,12] For example, a negative substrate bias voltage, V_b, can be applied to raise the energy of the positively charged ions that are bombarding the film surface during plasma assisted growth. In this way, the ion bombardment causes dehydrogenation by the preferential displacement of hydrogen atoms and allows for local reorganization of the carbon film microstructure to a denser material.[13] In a previous work[14] we reported that this approach yields fullerenelike (FL) arrangements, as detected by high resolution transmission electron microscopy. This structural transition coincides with a lower bulk hydrogen content and an improved wear resistance for $V_b < -100$ V. In another study,[15] we will present a detailed analysis of the mechanical and tribological properties of the *a*-C:H films.

II. EXPERIMENTAL SECTION

A. Film deposition

a-C:H films were grown by ECR-CVD (ASTEX, model AX4500) in a two-zone vacuum chamber operating with a 2.45 GHz microwave source at 208–210 W input power. Gas mixtures of methane/argon [15 SCCM/35 SCCM (SCCM denotes cubic centimeter per minute at STP)] were applied keeping the operating pressure at 1.1×10^{-2} Torr. Double-side polished *p*-type silicon (100) with a resistivity $>10\ \Omega$ cm and a thickness of 280 μm was used as substrate material. A dc bias varying from -300 to $+100$ V was directly applied to the silicon substrates while no intentional heating was employed. At the end of each 1 h deposition run the substrate temperature was evaluated by a thermocouple attached to the substrate holder. The thickness of the *a*-C:H films was determined with a Dektak 3030 profilometer by measuring the corresponding height differences produced by locally masking the substrate during film growth. In the range of bias values going from +100 toward -150 V the thickness increases progressively, while for biases more negative than -200 V a slightly lower thickness is observed. A maximum thickness of about 1130 nm is obtained for biases of -200 and -150 V.[16] It should be noted that the use of a dc bias might result in an effective bias, which is lower than the applied dc bias in the case of growing insulating *a*-C:H films. However, independent IR and Raman spectroscopy analyses do not show any changes in microstructure for layers up to 2–3 μm. Due to the much thinner films considered here, shielding of the applied dc voltage is discarded, as was also confirmed in previous work.[12] Also, possible differences in film density are not considered in this study.

B. Film characterization

The composition of the *a*-C:H films has been derived from ion beam analysis (IBA) techniques. In particular, simultaneous Rutherford backscattering spectrometry (RBS) and ERDA measurements were performed. The spectra were acquired by using a 2 MeV He^+ beam at an incidence angle of $\alpha = 75°$ with respect to the surface normal and using silicon surface barrier detectors located at scattering angles of 170° and 30° for detection of the backscattered projectiles and recoil atoms, respectively. In front of the forward detector, a 13-μm-thick Mylar foil was placed to filter the H recoils from heavier particles. The RBS and ERDA experimental spectra have been fitted using the same film structure by the SIMNRA code.[17] The cross section for the $^1H(\alpha,p)^4He$ process given by Quillet *et al.*[18] was used for quantification of the ERDA data.

XANES measurements were carried out at the dipole beamline PM4 using the SURICAT endstation of the synchrotron facility BESSY-II in Berlin, Germany. The samples were oriented with respect to the incident beam near the 55° magic angle in order to avoid orientational effects. The data were acquired in the total electron yield mode by recording the current drained to ground from the sample. Intensities were normalized to the signal recorded simultaneously from a gold covered grid. The resonance π^* peak from highly oriented pyrolitic graphite (HOPG) at 285.4 eV was used for energy calibration. IR absorption measurements were performed using a double-beam IR spectrophotometer (Hitachi 270–50) in the range from 1000 to 4000 cm^{-1}. Micro-Raman spectra were taken with a Renishaw Ramascope 2000 system with 514.5 nm Ar laser light.

Unfortunately, it was not possible to characterize the *a*-C:H films in the -90 to -140 V interval by ERDA and XANES due to problems associated with partial delamination of the films (about 2%–5% of the film area had been delaminated).

III. RESULTS AND DISCUSSION

A. Compositional analysis by ion beam analysis

Figure 1 shows the experimental RBS and ERDA (inset) spectra recorded simultaneously from an *a*-C:H film grown at $V_b = +100$ V. On the one hand, the RBS signal presents the contribution of backscattered He projectiles after collisions with O, C, and Si elements. The maximum energy from C and O corresponds to that given by the kinematic factor, indicating that they are present at the surface as film constituents. The yield is very low due to the reduced scattering cross section for low-Z elements and the low dose employed

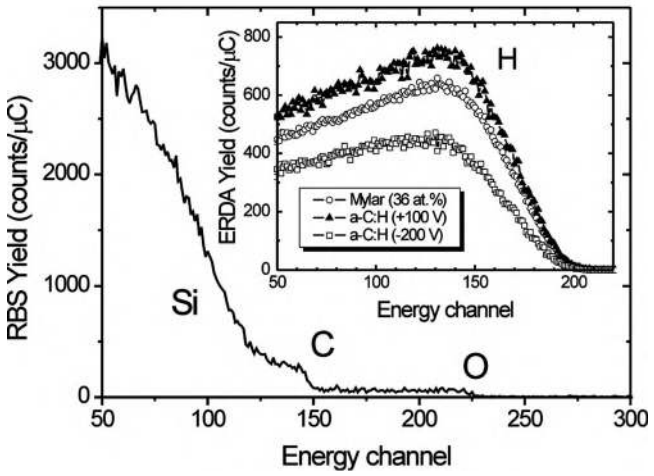

FIG. 1. RBS spectrum of the *a*-C:H film grown at an applied substrate bias, V_b, of +100 V. The inset shows the simultaneously recorded ERDA spectrum (closed triangles) together with ERDA spectra taken from the Mylar foil (open circles) and the *a*-C:H film grown at $V_b=-200$ V (open squares).

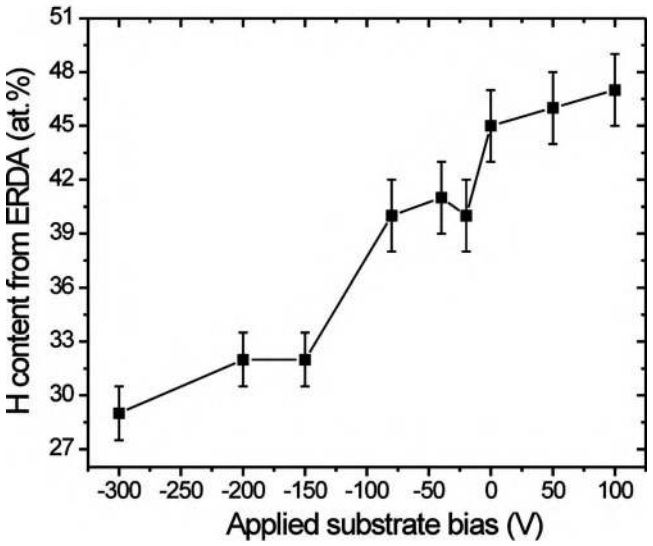

FIG. 2. ERDA H content of the *a*-C:H films as a function of the applied substrate bias voltage.

to avoid sample damage (H loss). In addition, note that the Si signal presents a broad onset, which might be related to the film surface roughness (~5 nm). However, it can also be partially due to the grazing incidence configuration and thickness inhomogeneity along the surface. Despite the high concentration of argon ions within the applied ECR plasma, RBS analysis of all *a*-C:H films shows that only a very limited number of argon ions (<1 at. %) is finally trapped within these films.

On the other hand, the ERDA spectrum (closed triangles) of the sample grown at $V_b=+100$ V shows the signal from H recoils after going through the range foil. The signal is plotted together with the yield obtained (for the same ion dose) from a Mylar foil (open circles) indicating the higher H content (>36 at. %) of the *a*-C:H film. The combination of RBS and ERDA analysis shows that the O contamination decreases for more negative bias (from 10 at. % at +100 V down to 1 at. % at −300 V) and that the H content decreases dramatically for high negative bias voltages ($V_b<-100$ V). For example, the ERDA spectrum of an *a*-C:H film deposited at $V_b=-200$ V (open squares) is well below those of the Mylar foil and the *a*-C:H film grown at $V_b=+100$ V. The trend in the H content is shown in Fig. 2. There is a progressive decrease in the hydrogen content toward more negative substrate bias and values ranging from 47 down to 29 at. % are derived showing a sharp drop around $V_b=-100$ V. The bias-induced hydrogen depletion during growth in the *a*-C:H film is likely induced by H and C atomic displacements that result in local recombination of atomic H and the formation of H_2 molecules. These molecules are either trapped in internal voids or diffuse to the surface and desorb.[19]

B. Infrared absorption spectroscopy

The optical absorption spectra (Fig. 3) obtained over the entire IR range investigated (4000–1000 cm^{-1}) display two main absorption regions.[9,16] The high-frequency band around 2900 cm^{-1} is related to different sp^3 C–H bond stretching vibrations (1–3), while the low-frequency structures from about 1800 to 1300 cm^{-1} can be separated into several contributions such as the sp^3 CH_3 symmetric bending (4), the sp^3 CH_2 scissors mode (5), and the sp^2 C=C double bond stretching (6) at about 1375, 1454, and 1600 cm^{-1}, respectively. The absorption peak at about 1700 cm^{-1} (7) can be assigned to the presence of C=O bonds. The feature observed around 2344 cm^{-1} (8) comes from the silicon wafer and is an artifact remnant of the double-beam collection method. Obviously, there are strong differences between the IR absorption spectra taken from the films grown from $+80\ V \geq V_b \geq -120$ V and those obtained at more negative substrate bias ($-150\ V \leq V_b \leq -300$ V). The first bias regime (upper four spectra in Fig. 3) is characterized by a strong absorption in the 2900 cm^{-1} range. The sp^3 CH_3 symmetric bending (4) and the sp^3 CH_2 scissors mode (5) can be observed as well. Analog to the detection of oxygen by RBS, the C=O absorption band at 1600 cm^{-1} (7) indicates a higher oxygen concentration for these *a*-C:H films, espe-

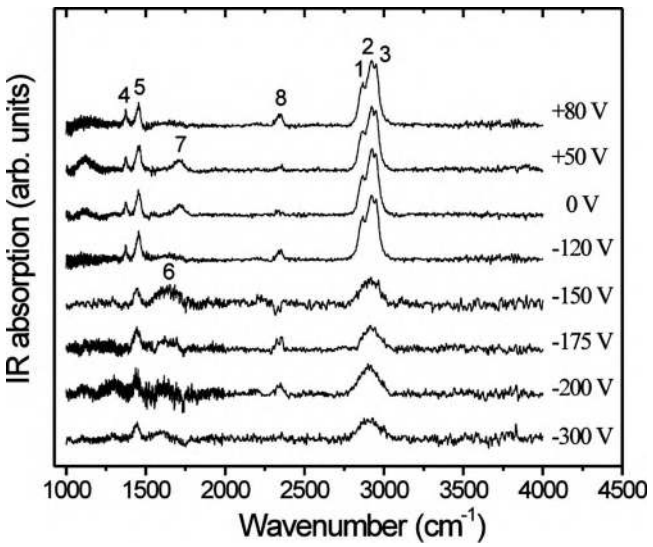

FIG. 3. Background subtracted IR absorption spectra of *a*-C:H films deposited with varying applied substrate bias.

cially for the films obtained at $V_b=0$ V and $V_b=+50$ V. For $V_b<-120$ V, however, the individual contributions (1–3) of the 2900 cm^{-1} band cannot be distinguished anymore. The symmetric bending of sp^3-CH_3 (4) cannot be detected either. The peak related to the stretching of C=C bonds at 1600 cm^{-1} (6) is strongest for $V_b=-150$ V and is found for the films deposited at highly negative bias only.

The line shape of the *a*-C:H films grown with +80 V $\geq V_b \geq -120$ V is very similar and the appearance of three contributions in the high-frequency band is typical for these so-called PLCH films, which contain polymerlike hydrocarbon chains with relatively little cross-linking between these chains. For $V_b<-120$ V, the high-frequency band (1–3) becomes less pronounced and the different $CH_{2,3}$ stretching vibrations cannot be distinguished as separate peaks. Also, the overall intensity of the 2900 cm^{-1} band decreases for increasing ion energy, indicative for the ion-induced hydrogen depletion of the produced *a*-C:H films. Although in earlier works[9,20–22] decomposition of the 2900 cm^{-1} band was performed by multiple stretching modes (even up to ten), the high-frequency band can be considered as the sum of mainly three different contributions[9] and, therefore, it is here fitted by three Gaussians only. The high-frequency stretching modes centered at around 2876 (1), 2921 (2), and 2954 cm^{-1} (3) can be assigned to the in-phase (symmetric) CH_3, out-of-phase (asymmetric) CH_2, and out-of-phase (asymmetric) CH_3 stretching vibrations, respectively. The total area under the 2900 cm^{-1} band (the IR signal being recorded in absolute intensity) is a relative measure for the content of bonded H in the *a*-C:H films.

Note that hydrogen can be bonded to sp^3- or sp^2-hybridized C sites, but since no IR components are centered around 3000 and 3050 cm^{-1}, i.e., at the positions of the stretching vibrations of olefinic and aromatic sp^2-CH groups,[9,22] and the IR signal does not extend much beyond 3000 cm^{-1}, we might conclude that for our *a*-C:H films hydrogen is preferentially bonded to sp^3-hybridized C atoms. This is in full agreement with earlier solid state NMR investigations[23] of *a*-C:H films grown by dc plasma assisted CVD where no sp^2 C–H could be identified at all.

C. Visible Raman spectroscopy

The visible Raman spectra of *a*-C:H films deposited at varying V_b are displayed in Fig. 4(a). For reasons of clarity, the collected spectral data have been multiplied by different factors in order to produce an ordered stacking of spectra without altering the peak positions or ratio of peak intensities. Neglecting the silicon substrate peak at 520 cm^{-1} that is observed for all *a*-C:H films deposited with -80 V $\leq V_b \leq$ +80 V, the Raman spectra of these films are rather featureless. They display a strong PL that is related to the hydrogen saturation of nonradiative recombination centers.[10,24] For the *a*-C:H films grown with -300 V $\leq V_b \leq -80$ V, the so-called *D* and *G* peaks, at about 1350 and 1580 cm^{-1}, respectively, become visible. The second order signals of these *D* and *G* peaks are located around 3000 cm^{-1}. The *G* peak is due to the bond stretching of all pairs of sp^2 carbon atoms in both rings and chains.[3] The *D* peak is a disorder-induced band that appears due to a double-resonance Raman process and results from the breathing modes of sp^2 carbon atoms in rings.[25]

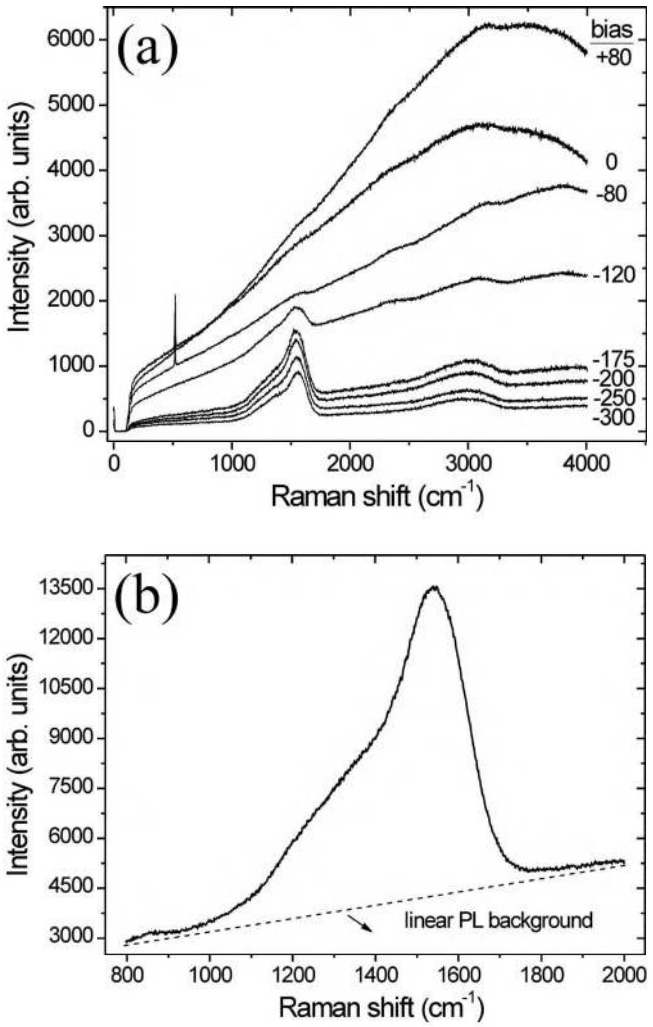

FIG. 4. (a) Raman spectra of *a*-C:H films deposited with varying applied substrate bias voltages (in volts). (b) Raman signal of the *a*-C:H film grown at $V_b=-175$ V with indicated linear PL background.

Semiquantitative information about the H content of the *a*-C:H films deposited at $V_b \leq -80$ V can also be obtained from these single-wavelength (514.5 nm) Raman spectra by measuring the slope of the PL background.[10] In this work, the PL background (given in microns) is calculated as the ratio between the slope *m* of the spectral background, measured between 800 and 2000 cm^{-1}, normalized to the maximum intensity (height) of the Raman *G* peak $[I(G)]$.[10] For simplicity, a linear background has been considered as shown in Fig. 4(b) for the Raman spectrum of an *a*-C:H film deposited at $V_b=-175$ V. After subtraction of this linear background, the *D* and *G* peaks are fitted with two Gaussians. For the *a*-C:H samples grown with $V_b>-80$ V, the *G* and *D* bands are overshadowed by the strong PL. Therefore, $m/I(G)$ can only be derived from the *a*-C:H samples grown in the bias range -300 V $\leq V_b \leq -80$ V.

D. X-ray absorption near edge spectroscopy

In Fig. 5, the C(1*s*) XANES spectra of *a*-C:H films produced at various V_b are shown, all of them normalized to

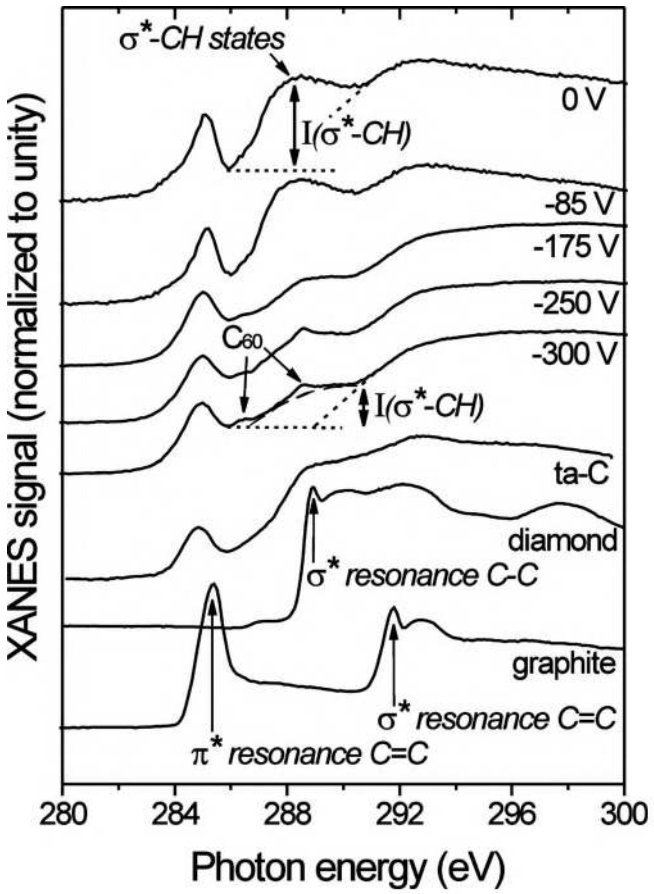

FIG. 5. C(1*s*) XANES spectra of *a*-C:H films deposited with varying applied substrate bias. The reference spectra of HOPG, diamond, and ta-C are added in the lower part of the figure. The determination of the intensity of the σ^*(C–H) states, $I(\sigma^*\text{-CH})$, is indicated for the *a*-C:H films grown at $V_b=0$ V and $V_b=-300$ V.

unity. The reference spectra of HOPG, diamond, and H-free tetrahedral amorphous carbon (ta-C) normalized to unity are added for comparison. The diamond reference spectrum exhibits a single absorption edge corresponding to the onset of transitions from the core level to the unoccupied σ^* states, with a maximum intensity in the region between 289 and 293 eV. The HOPG reference spectrum shows two absorption edges, the higher energy one corresponding to $1s \rightarrow \sigma^*$ transitions, with maximum intensity between 292 and 294 eV, and the lower energy band corresponding to $1s \rightarrow \pi^*$ transitions with an onset at ~285 eV. The ta-C reference is added as a reference of a H-free, disordered carbon material with dominant sp^3 character and reduced intensity in the π^* region.

The spectra of the *a*-C:H films grown at $V_b=0$ V and $V_b=-85$ V show some similarities with that from ta-C, but with an increased intensity at 288.0 eV due to the contribution of σ^* C–H states.[14,26] Also, the π^* peak from the sp^2 hybrids is sharper than the corresponding peak in ta-C. Like we already demonstrated in previous work,[14] for the *a*-C:H films deposited with $V_b<-100$ V there are three main apparent changes in the XANES line shape as compared to the samples grown at $V_b>-100$ V: (i) the π^* peak is broader, (ii) the CH peak is reduced, and (iii) there are new, relatively low intensity peaks appearing at 286.0 and 288.5 eV, for example. These latter peaks match exactly at the positions of the LUMO+1 and the LUMO+3 states of molecular C_{60}.[27] This indicates the self-formation of C_{60} inclusions and FL arrangements during the film growth process.

Although in principle there are subtle changes in the shape of the σ^*-CH states in the presence of different local environments of the hybridized C atom, all features appear in the same energy region (~287.5 eV). The XANES intensity related to the σ^*-CH states, $I(\sigma^*\text{-CH})$, at 287–290 eV is, therefore, a relative measure of the content of bonded hydrogen within the *a*-C:H films. In Fig. 5 the assessment of the intensity of the C–H band is illustrated for the *a*-C:H films grown at $V_b=0$ V and $V_b=-300$ V, respectively. Whereas the determination of the signal from the σ^*-CH states is rather straightforward for the sample grown at 0 V, the minor signals coming from the self-formed C_{60} inclusions[14] slightly complicate the direct assessment of $I(\sigma^*\text{-CH})$ for the films deposited with $V_b<-100$ V. Nevertheless, $I(\sigma^*\text{-CH})$ can be estimated well by extrapolation of the broad σ^* band edge starting at around 290.8 eV and the π^* C=C absorption at around 285.8 eV, as is illustrated in Fig. 5 for the case of $V_b=-300$ V. Due to the initial normalization to unity of the XANES spectra, the intensity $I(\sigma^*\text{-CH})$ will be always smaller than 1.

E. Comparison of spectroscopic techniques

Figure 6 shows the correlation between the (absolute) H content measured by ERDA and the relative signal obtained for spectral features by IR, visible Raman, and XANES spectroscopies. From these correlations, we have derived empirical, semiquantitative relationships to calculate the hydrogen content [H] in *a*-C:H films.

In Fig. 6(a), the 2900 cm^{-1} IR band area (absorbance) normalized to the *a*-C:H film thickness (in microns), $\bar{A}_{IR}$, is plotted as a function of the ERDA hydrogen content. There is a fairly strong linear correlation between these data as, obviously, $\bar{A}_{IR}$ increases linearly with the ERDA hydrogen content. The coefficient of regression, R^2, is 0.91 [linear best fit indicated by dashed line in Fig. 6(a)]. For the hydrogen content, $[H]_{IR}$, the following expression is then obtained:

$$[H]_{IR} = 23.2 + 20\bar{A}_{IR}. \quad (1)$$

The slope (0.05/at. %) of the linear fit in Fig. 6(a) is rather high, because $\bar{A}_{IR}$ drops by a factor of about 3 for the *a*-C:H films containing 47–29 at. % hydrogen, respectively. This discrepancy can be assigned to several factors: (i) the transition dipole moments (or absorption strengths) of the individual C–H vibrations are not identical and depend on the specific microstructure of the *a*-C:H films,[22,28] (ii) it is assumed that all hydrogen measured by ERDA is bonded to carbon atoms, and (iii) the IR absorption was not corrected for reflection losses.

Figure 6(b) shows the PL background, $m/I(G)$, derived from the visible Raman spectra (Fig. 4) of the *a*-C:H films grown with $V_b \leq -80$ V as a function of the ERDA hydrogen content. The values of $m/I(G)$ displayed in closed squares are from *a*-C:H films deposited at V_b values of −300, −200, −175, and −80 V. For these samples the hydrogen content

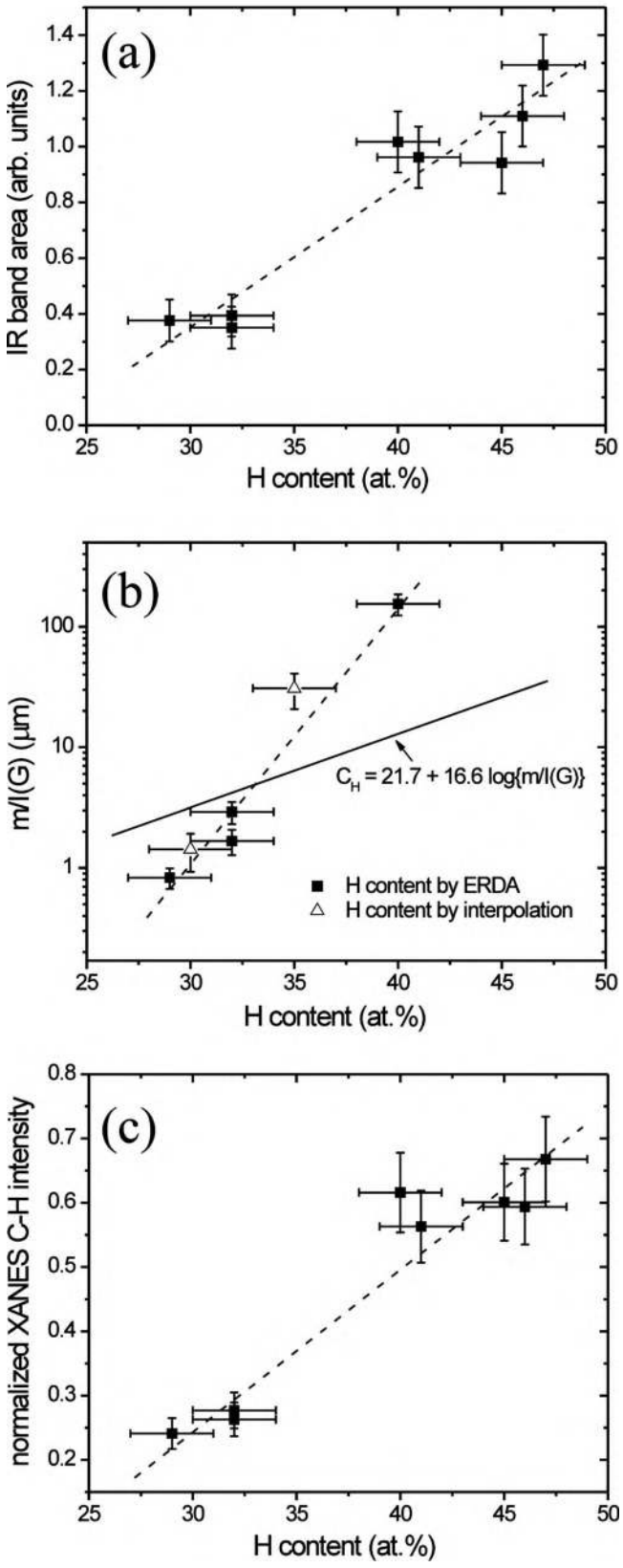

FIG. 6. Correlation between hydrogen content measured by ERDA and (a) the normalized IR (C–H) band area at about 2900 cm^{-1}, (b) the Raman PL background, and (c) the XANES σ^*-CH band intensity. The dashed lines represent the linear best fits through the data points from which the empirical expressions (1), (2), and (4) are derived (see text). The closed squares, open triangles, and solid line in (b) represent the four data points obtained by ERDA directly, the two data points obtained by interpolation of the ERDA data in Fig. 2, and the expression between PL background and hydrogen content (3) found by Casiraghi *et al.* (Ref. 10), respectively.

was measured directly by ERDA. The $m/I(G)$ values for the a-C:H films grown at $V_b=-250$ V and $V_b=-120$ V are shown with open triangles since the H content was here obtained by interpolation of the ERDA data of Fig. 2 (no direct ERDA data were available for these a-C:H films). The PL background, plotted in logarithmic scale, scales linearly with the H content. The dashed line in Fig. 6(b) shows the linear best fit through the data points ($R^2=0.94$) and from it we can deduce

$$[\mathrm{H}]_{\mathrm{Raman}} = 30.0 + 4.6 \log\{m/I(G)\}. \quad (2)$$

In a previous study, Casiraghi *et al.*[10] derived a semiquantitative estimation of the hydrogen content, ${}^{\mathrm{C}}[\mathrm{H}]_{\mathrm{Raman}}$, for a larger selection of a-C:H films produced with different techniques and gas precursors

$${}^{\mathrm{C}}[\mathrm{H}]_{\mathrm{Raman}} = 21.7 + 16.6 \log\{m/I(G)\}. \quad (3)$$

This relation is represented by the solid line in Fig. 6(b). There is a large deviation between our correlation [Eq. (2)] and that derived by Casiraghi *et al.*[10] [Eq. (3)]. This might be explained by the limited number of data points in our study, the limited range of hydrogen contents (20–45 at. %) on which Eq. (3) was based[10] and/or the fact that the PL background in the Raman spectra is not perfectly linear.

In Fig. 6(c), the intensity of the XANES σ^*-CH band, $I(\sigma^*\text{-CH})$, is given as a function of the ERDA hydrogen content. Again, there is a strong linear correlation between the plotted data, as $I(\sigma^*\text{-CH})$ increases linearly with the ERDA hydrogen content. $I(\sigma^*\text{-CH})$ now drops by a factor of about 2.5 for the a-C:H films containing 47 and 29 at. % hydrogen, respectively. For the linear best fit indicated by the dashed line in Fig. 6(c), $R^2=0.98$. The empirical relation between the XANES σ^*-CH intensity and hydrogen content, $[\mathrm{H}]_{\mathrm{XANES}}$, can then be written as

$$[\mathrm{H}]_{\mathrm{XANES}} = 20.4 + 39.6 I(\sigma^*\text{-CH}). \quad (4)$$

Remarkably, the trends for the XANES σ^*-CH intensity [Fig. 6(c)] and IR CH_x stretching band area [Fig. 6(a)] as a function of the ERDA hydrogen content are very similar. Although both techniques IR and XANES are based on the detection of C–H bonds, they differ significantly, not only in the process of C–H bond detection and sensitivity but also in the detection range. IR absorption spectroscopy in transmission mode detects C–H bonds in the bulk, whereas XANES is a surface sensitive technique with absorption signals coming from the surfacemost 5–10 nm. Nevertheless, the strong correlation between the IR and XANES data shows that their quantification data for hydrogen can be taken as roughly representative of bulk composition, similar to that found in previous work by Yubero *et al.*[6,8] for the determination of the hydrogen content by the surface sensitive REELS technique.

A very striking point is that for a negligible intensity of the IR 2900 cm^{-1} and XANES σ^*-CH bands as well as an almost flat PL background (i.e., with $\log\{m/I(G)\}\sim 0$) Eqs. (1), (4), and (3), respectively, yield [H] ~20 at. %. This result can be explained either considering that the above expressions are only valid in the H concentration explored, i.e., 29–47 at. %, or alternatively that the amount of hydrogen contained in the film and not bound to carbon, presumably in

the form of –OH bonds or H_2 and H_2O molecules dispersed in voids, is around 20 at. %. This might especially be the case for the *a*-C:H films with the highest O concentration and lowest film density, i.e., the polymerlike films deposited at positive or less negative bias. However, the absence of these oxygen-related vibrational and/or electronic states in the measured IR and XANES spectra (Figs. 3 and 5) indicates a minor effect of oxygen on the bonding characteristics of the *a*-C:H films. Moreover, although several studies[20,22,23] indicate that a significant fraction of the total hydrogen amount in *a*-C:H films can be unbound, it is generally accepted that this fraction is rather low. Nevertheless, our results indicate that the combination of spectroscopic studies sensitive to H bound to C, with techniques sensitive to the total H content, can solve the quantification of the ratio of bound/unbound hydrogen in *a*-C:H films, provided a complete enough set of samples with low (1–5 at. %) and high (~50 at. %) H contents.

IV. CONCLUSIONS

Four spectroscopic techniques were employed to assess the dehydrogenation of *a*-C:H films produced by bias-enhanced ECR-CVD. By changing the dc substrate bias from +100 V down to −300 V, drastic changes in the hydrogen content and microstructure of the *a*-C:H films are observed. This work shows that hydrogen release mechanisms are very effective. PLCH films containing large amounts of bonded hydrogen (40–47 at. %) are deposited under positive or low negative bias voltages, whereas the hydrogen content drops well below 35 at. % and hard *a*-C:H films are obtained for high negative bias conditions (<−100 V). Using ERDA as a reference technique to determine absolute values for the H content, we have deduced semiquantitative expressions to estimate the hydrogen content in *a*-C:H materials from the relative signal of characteristic spectroscopic parameters such as the integrated area of the IR C–H stretching band at about 2900 cm^{-1}, the PL background in visible Raman spectra, and the XANES σ^*-CH intensity.

ACKNOWLEDGMENTS

This work has been partially financed by the project FOREMOST (Contract No. NMP3-CT-2005-515840) from the EU FP6 program and FIS2006-12253-C06-02 and MAT2006-13006-C02-01 from MEC (Spain). The synchrotron work at BESSY-II was supported by the EU under Contract No. R II 3-CT-2004-506008. J.G.B. and M.C. acknowledge financial support from the Juan de La Cierva program (MEC, Spain) and the Dutch Veni grant, and from the CSIC, respectively.

[1] J. Robertson, Mater. Sci. Eng., R. **37**, 129 (2002).
[2] A. C. Ferrari and J. Robertson, Phys. Rev. B **61**, 14095 (2000).
[3] C. Casiraghi, A. C. Ferrari, and J. Robertson, Phys. Rev. B **72**, 085401 (2005).
[4] S. Sattel, J. Robertson, and H. Ehrhardt, J. Appl. Phys. **82**, 4566 (1997).
[5] L. F. Xia and M. R. Sun, J. Inorg. Mater. **17**, 777 (2002).
[6] F. Yubero, V. J. Rico, J. P. Espinós, J. Cotrino, and A. R. González-Elipe, Appl. Phys. Lett. **87**, 084101 (2005).
[7] S. Takabayashi, K. Okamoto, H. Sakaue, T. Takahagi, K. Shimada, and T. Nakatani, J. Appl. Phys. **104**, 043512 (2008).
[8] V. J. Rico, F. Yubero, J. P. Espinós, J. Cotrino, A. R. González-Elipe, D. Garg, and S. Henry, Diamond Relat. Mater. **16**, 107 (2007).
[9] Y. Bounouh, M. L. Thèye, A. Dehbi-Alaoui, A. Matthews, and J. P. Stoquert, Phys. Rev. B **51**, 9597 (1995).
[10] C. Casiraghi, F. Piazza, A. C. Ferrari, D. Grambole, and J. Robertson, Diamond Relat. Mater. **14**, 1098 (2005).
[11] P. Reinke, S. Schelz, W. Jacob, and W. Möller, J. Vac. Sci. Technol. A **10**, 434 (1992).
[12] P. Reinke, W. Jacob, and W. Möller, J. Appl. Phys. **74**, 1354 (1993).
[13] J. Robertson, Diamond Relat. Mater. **3**, 361 (1994).
[14] J. G. Buijnsters, M. Camero, R. Gago, A. R. Landa-Canovas, C. Gómez-Aleixandre, and I. Jiménez, Appl. Phys. Lett. **92**, 141920 (2008).
[15] J. G. Buijnsters, M. Camero, L. Vázquez, F. Agulló-Rueda, R. Gago, I. Jiménez, C. Gómez-Aleixandre, and J. M. Albella (unpublished).
[16] J. G. Buijnsters, M. Camero, L. Vázquez, F. Agulló-Rueda, C. Gómez-Aleixandre, and J. M. Albella, Vacuum **81**, 1412 (2007).
[17] M. Mayer, "SIMNRA User's Guide," IPP Report No. 9/113, 1997.
[18] V. Quillet, F. Abel, and M. Schott, Nucl. Instrum. Methods Phys. Res. B **83**, 47 (1993).
[19] D. Liu, J. Zhang, Y. Liu, J. Xu, and G. Benstetter, J. Appl. Phys. **97**, 104901 (2005).
[20] G. Fanchini, P. Mandracci, A. Tagliaferro, S. E. Rodil, A. Vomiero, and G. Della Mea, Diamond Relat. Mater. **14**, 928 (2005).
[21] B. Dischler, in *Amorphous Hydrogenated Carbon Films*, EMRS Symposia Proceedings, edited by P. Koidl and P. Oelhafen (Les Éditiones de Physique, Paris, 1987), Vol. 17, p. 189.
[22] J. Ristein, R. T. Stief, L. Ley, and W. Beyer, J. Appl. Phys. **84**, 3836 (1998).
[23] C. Donnet, J. Fontaine, F. Lefèbvre, A. Grill, V. Patel, and C. Jahnes, J. Appl. Phys. **85**, 3264 (1999).
[24] J. Robertson, Phys. Rev. B **53**, 16302 (1996).
[25] C. Thomsen and S. Reich, Phys. Rev. Lett. **85**, 5214 (2000).
[26] C. Ziethen, O. Schmidt, G. K. L. Marx, G. Schönhense, R. Frömter, J. Gilles, J. Kirschner, C. M. Schneider, and O. Gröning, J. Electron Spectrosc. Relat. Phenom. **107**, 261 (2000).
[27] M. Nyberg, Y. Luo, L. Triguero, L. G. M. Pettersson, and H. Ågren, Phys. Rev. B **60**, 7956 (1999).
[28] W. Jacob and M. Unger, Appl. Phys. Lett. **68**, 475 (1996).